

Microlens diagnostics of accretion disks in active galactic nuclei

A. Yonehara¹, S. Mineshige¹, J. Fukue², M. Umemura³, and E.L. Turner⁴

¹ Department of Astronomy, Kyoto University, Sakyo-ku, Kyoto 606-8502, Japan

² Astronomical Institute, Osaka Kyoiku University, Asahigaoka, Kashiwara, Osaka 582-0026, Japan

³ Center for Computational Physics, Tsukuba University, Tsukuba, Ibaraki 305-0006, Japan

⁴ Princeton University Observatory, Peyton Hall, Princeton, NJ 08544

June 14, 2019

Abstract. The optical-ultraviolet continuum from active galactic nuclei (AGN) seem to originate from optically thick and/or thin disks, and occasionally from associated circumnuclear starburst regions. These different possible origins can, in principle, be discriminated by observations of gravitational microlensing event. We performed numerical simulations of microlensing of an AGN disk by a single lensing star passing in front of the AGN. Calculated spectral variations and light curves show distinct behavior, depending on the nature of emitting region; the time variation of a few months with strong wavelength dependence is expected in the case of an optically thick disk (*standard disk*), while an optically thin disk (*advection-dominated disk*) will produce shorter, nearly wavelength-independent variation. In the case of a starburst region much slower variations (over a year) will be superposed on the shorter variations.

Key words: accretion, accretion disks — active galactic nuclei — microlensing

1. Introduction

There has been long discussion regarding the central structure of active galactic nuclei (AGN). Generally, it is believed that there is a supermassive black hole and a surrounding accretion disk. However, it is quite difficult to obtain direct information about the center of AGN, the accretion disk, because the disk size is far too small to resolve. As for Q2237+0305, for example, the angular diameter distance is $\sim 4 \times 10^{27}$ cm. If a black hole placed at the center has a mass of $\sim 10^8 M_\odot$, the disk size ($\sim 1000 r_g$,

r_g is Schwarzschild radius) will be $\sim 3 \times 10^{16}$ cm. Hence, apparent disk size is $\sim 10^{-11}$ radian $\sim 1 \mu$ as

What is usually done is to observe the spectra, which are integrated over the entire regions, and to make a fitting to the observed spectra by theoretical integrated spectra. However, there remain ambiguities related with the spatial distribution of local spectra. The standard picture is that the so-called UV bump is attributed to blackbody radiation from the standard-type, optically-thick disks (e.g., Shakura & Sunyaev 1973). Such a fundamental belief may be reconsidered by the recent HST observations that show no big blue bumps (e.g., Zheng et al. 1997).

Instead, microlensing can be used as a ‘gravitational telescope’ to resolve the disk structure (see Blandford & Hogg 1995; originally proposed by Chang & Refsdal 1984), since a typical Einstein-ring radius of a stellar mass lens is very small; e.g., $\theta_E \sim 10^{-11}$ radian for Q2237+0305. With such a gravitational telescope we can obtain information about the disk emergent spectra as a function of the distance from the central black hole. When a point source object is lensed, its luminosity is amplified without any color change (this feature is called ‘achromaticity’) and there have been many literatures discussing these events, initiated by Paczyński (1986; for a review see Narayan & Bartelmann 1996). But, in some actual situations, we cannot treat a source as a point and the effect of a finite source size should be taken into account. Grieger, Kayser & Refsdal (1988) examined such finite size effects. They simulated microlensing light curves for two different source profiles: stellar like and accretion disk like. The light curves show different shapes from those of point source calculations. However, they only considered monochromatic intensity. Furthermore, Wambsganss & Paczyński (1991) pointed out that if the finite size source has inhomogeneous structure, so that each part produces a different spectrum, lensing light curves have wavelength dependence; i.e., chromatic features in microlensing events

Send offprint requests to: A. Yonehara

* e-mail: yonehara@kusastro.kyoto-u.ac.jp

should appear. But, in their illustrative simulations, only a few parts with different colors are considered. Using this chromatic effect, several authors calculated microlensing light curves of AGN accretion disk based on simple disk models (e.g., Rauch & Blandford 1991; Jaroszyński, Wambsganss & Paczyński 1992).

The purpose of this paper is to obtain some criteria for distinguishing disk physics based on more realistic disk models: an optically-thick, standard-type disk and an optically-thin, advection dominated disk. For this purpose, we, for the first time, adopt the most successful, optically thin disk models, the advection-dominated accretion flow (ADAF; Narayan & Yi 1995; Abramowicz et al. 1995). So far nobody has yet calculated X-ray or radio emission in the microlens events, due probably to the lack of reliable disk models. However, such calculations are of great importance since X-ray and radio emission seems to originate from the vicinity of a putative black hole. In section 2 we describe our methods of simulation. In section 3 our results are displayed. Section 4 is devoted to discussion.

2. Method of the simulation

2.1. Accretion disk models

First, we describe the adopted accretion disk models. We consider two representative types of disks:

1. An optically thick disk:

The first case we consider is the geometrically-thin and optically-thick standard disk (Shakura & Sunyaev 1973). Since we are concerned with disk structure on scales ranging from a few tens to a few thousands of r_g , we ignore relativistic effects, such as the gravitational redshift by the black hole, for simplicity. The temperature distribution of the optically thick standard disk is then given by (Shakura & Sunyaev 1973)

$$T(r) = 2.2 \times 10^5 \left(\frac{\dot{M}}{10^{26} \text{ g s}^{-1}} \right)^{1/4} \left(\frac{M}{10^8 M_\odot} \right)^{1/4} \times \left(\frac{r}{10^{14} \text{ cm}} \right)^{-3/4} \left[1 - \left(\frac{r_{\text{in}}}{r} \right)^{1/2} \right]^{1/4} \text{ K}, \quad (1)$$

where \dot{M} is the mass accretion rate and M is the black hole mass. The inner edge of the disk, r_{in} , is set to be $r_{\text{in}} = 3r_g$, the radius of the marginally stable last circular orbit around a non-rotating black hole.

Since the disk is optically thick, we can assume black-body radiation. Inserting the temperature profile $T(r)$ into

$$\Delta L(\nu, r) = 2 \cdot 4\pi B_\nu [T(r)] \Delta S \cos i, \quad (2)$$

we can calculate luminosity at radius r and frequency ν , where B_ν is a Planck function, $\Delta S = \Delta r \cdot r \Delta \varphi$ is the surface element on the disk plane and i is the inclination angle

of the disk. For simplicity, here, we assume the disk is face-on ($i = 0$). It might be noted that the radiation spectra do not depend on the viscosity in this standard-type disks, since the total emissivity and the effective temperature is solely determined by the energy balance between the radiative cooling and viscous heating (which originates from gravitational energy release).

2. An optically thin disk

The second model is the optically thin version of the advection dominated accretion flow (ADAF). We used the spectrum calculated by Manmoto, Mineshige, & Kusunose (1997) and derive luminosity $\Delta L(\nu, r)$ in the same way as for an optically thick disk (details are given in Manmoto et al. 1997):

$$\Delta L(\nu, r) = 2 \cdot \epsilon_\nu(r) \Delta S, \quad (3)$$

where ϵ_ν is emissivity. In this calculation, we used the emissivity for face-on disk. Here, included are synchrotron, bremsstrahlung, and inverse Compton scattering of soft photons created by the former two processes (see Narayan & Yi 1995 for more details). Optical flux is mainly due to Comptonized synchrotron photons.

In this sort of disks (or flows), radiative cooling is inefficient because of very low density. As a result, accreting matter falls into a central object, hardly losing its internal energy (which is converted from its gravitational energy through the action of viscosity) in a form of radiation. Hence, although the total disk luminosity is less than that of the standard one for the same mass-flow rate, the disk can be significantly hotter, with electron temperatures being of the order of 10^9 K or more, thus producing high energy (X- γ ray) photons. Photon energy is thus widely spread over large frequency ranges. Since emission inside the last circular orbit (at $3r_g$) is not totally negligible in this case, we solve the flow structure until the event horizon (r_g) passing through the transonic point, and consider radiation from the entire region outside the horizon, although the contribution from the innermost part is not dominant. Unlike the optically thick case, the viscosity explicitly affects the emissivity in this case, since radiative cooling is no longer balanced with viscous heating (and with gravitational energy release). In the present study, we assign the viscosity parameter to be $\alpha = 0.1$.

2.2. Microlensing events

Generally, the microlensed images are split into two (or more) images. When the image separation is too small for observers to resolve, however, the total magnitudes of all the split images vary due to this microlensing.

The properties of microlensing have been extensively examined for simple cases where both the lens and source are regarded as being point source (e.g., Paczyński 1986).

The total amplification (or magnification) factor A for microlensing is exactly expressed as

$$A(u) = \frac{u^2 + 2}{u(u^2 + 4)^{1/2}}, \quad (4)$$

where u corresponds to the angular separation between lens and source in the units of the Einstein ring radius and is, of course, a function of the relative distance between the lens and the source.

Here, the Einstein ring radius is

$$\theta_E = \left(\frac{4GM_{\text{lens}}}{c^2} \frac{D_{\text{ls}}}{D_{\text{os}}D_{\text{ol}}} \right)^{1/2} \quad (5)$$

where M_{lens} is the mass of a lensing star, c is the speed of light, G is the gravitational constant, and D_{ls} , D_{os} , and D_{ol} denote the angular diameter distances from lens to source, from observer to source, and from observer to lens, respectively (Paczynski 1986). Adopting an appropriate cosmological model, we can calculate these angular diameter distances in terms of redshifts z_{ls} (from lens to source), z_{os} (from observer to source), and z_{ol} (from observer to lens). In the present study, we assume the Einstein-de Sitter Universe, in which we have

$$D_x = \frac{2c}{H_0} \frac{1}{1+z_x} \left[1 - \frac{1}{(1+z_x)^{1/2}} \right], \quad (6)$$

where H_0 is Hubble's constant, and the subscript 'x' stands for 'ls', 'os', or 'ol'.

Since we now consider microlensing effects on an extended source, we must integrate the magnification effects over the entire source. We thus, as a next step, need to calculate the angular separation u between a part of the source in question and the lens center, from which the amplification factor, $A(u)$, can be found. In the present study, we first divide an accretion disk plane into azimuthal (φ) and radial (r) elements. The azimuthal coordinate is equally divided into ~ 1000 segments (φ_i), while the logarithmically scaled radial coordinate is also equally divided into ~ 1000 segments (r_j). We then calculate the observed flux at frequency ν from a cell between r_j and r_{j+1} in the radial direction and between φ_i and φ_{i+1} in the azimuthal direction. Noting that photons emitted by the source at a frequency ν are observed at the frequency $\nu/(1+z_{\text{os}})$, we write the observed flux as

$$\Delta F_{\text{obs}}(\nu; r_j, \varphi_i) \simeq A(u) \Delta F_{\text{obs},0}[\nu(1+z_{\text{os}}), r_j], \quad (7)$$

where $A(u)$ is the amplification factor given by equation (4). Moreover, u is explicitly given by

$$u = \left[(r \cos \varphi - r_{\text{lens}} \cos \varphi_{\text{lens}})^2 + (r \sin \varphi - r_{\text{lens}} \sin \varphi_{\text{lens}} \cos i)^2 \right]^{1/2} \theta_E^{-1}, \quad (8)$$

where i is the inclination angle of an accretion disk, and r_{lens} and φ_{lens} represent the radial and the azimuthal

positions of the lens in units of radians, respectively. The intrinsic flux in the absence of a microlensing event, $\Delta F_{\text{obs},0}(\nu, r)$, is calculated from $\Delta L(\nu, r)$ according to

$$\Delta F_{\text{obs},0}(\nu, r) = \frac{\Delta L(\nu, r)}{4\pi D_{\text{os}}^2 (1+z_{\text{os}})^3}, \quad (9)$$

and $\Delta L(\nu, r)$ was given in §2.1.

Summing up $\Delta F_{\text{obs}}(\nu; r, \varphi)$ over the entire disk plane from the inner boundary (r_{in}) to the outer boundary (r_{out}), we obtain the total observed flux at frequency ν , or the spectrum of the microlensed accretion disk.

3. Results of the calculations

3.1. Model parameters

For clarity, we consider a lensed quasar, Q 2237+0305 (the Einstein cross, e.g., Huchra et al. 1985), Irwin et al. (1989) reported an increase of the apparent luminosity of image A by ~ 0.5 mag on a timescale of a few months, which was nicely reproduced by a model of microlensing (Wambsganss, Paczyński, & Schneider 1990). At present, at least five microlens events have been reported so far on the split images (Irwin et al. 1989; Corrigan et al. 1991; Houde & Racine 1994). Although it is not always clear whether microlensing by a single object is a good approximation for Q 2237+0305 itself (see discussion), we just take this object as one test case and derive quite general conclusions regarding the general observational features of microlensed accretion disks.

This object is macrolensed by a foreground galaxy, and the source is split into four (or five) images. Now, we suppose that one of the macrolensed image is further microlensed by a star in the foreground galaxy causing the microlensing. Although the macrolensed images are actually affected by two effects, so called, 'convergence' and 'shear', we here neglect both for simplicity and thus assume that the macrolensed image is neither amplified nor distorted. The redshift parameters are

$$z_{\text{os}} = 1.675, \quad z_{\text{ol}} = 0.039, \quad \text{and} \quad z_{\text{ls}} = 1.575 \quad (10)$$

(cf. Irwin et al. 1989). As for Hubble's constant, we adopt the approximate value obtained by Kundić et al. (1997), $H_0 \sim 60 \text{ km s}^{-1} \text{ Mpc}^{-1}$. The adopted disk parameters are the outer edge of the disk, $r_{\text{out}} = 10^3 r_g$, the mass of the central black hole, $M = 10^8 M_{\odot}$, and the mass-flow rates, $\dot{M} = 10^{26} \text{ g s}^{-1}$ for the standard disk and $\dot{M} = 10^{22} \text{ g s}^{-1}$ for the optically thin disk. We take different mass-flow rates for two cases because of calculation convenience. This is not, fortunately, a serious problem, since it has been demonstrated that the spectral shape of the ADAF is not very sensitive to \dot{M} , although the overall flux level does change. We will not discuss the absolute flux in the following discussion, and focus on the relative spectral shape and relative flux variation. For other basic parameters characterizing the disks, see §2.1.

For simplicity, we assume that the accretion disk is face-on; i.e. $i = 0$, to the observer. Actually, based upon a grand unified paradigm of AGNs, quasars are not far from face-on views. We also assume the mass of a lensing object to be $M_{\text{lens}} = 1.0M_{\odot}$ or $0.1M_{\odot}$. The remaining variable is the angular separation (u) between the lens and a part of the source in question.

3.2. Spectral variation

First, we calculated the microlensed spectra of each of two types of accretion disks for the angular separation between the lens and the source of $u = 1.0, 0.1$, and 0.01 , respectively. The results are shown in figure 1 for the standard disk (in the upper panel) and for the optically thin disk (in the lower panel), respectively. For the former disk not

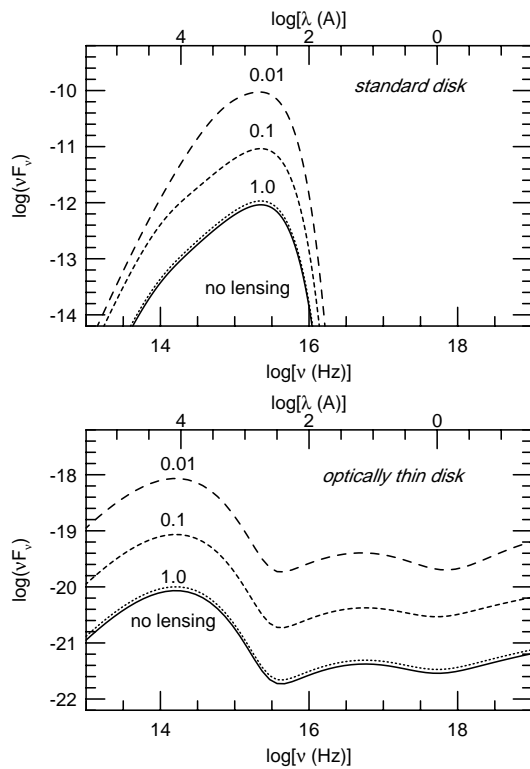


Fig. 1. Microlensed spectrum of a standard accretion disk (upper) and an optically thin accretion flow (lower). In each panel, the microlensed spectra are plotted for angular separations between the disk center and the lensing star to be $u = 1.0$ (dotted line), 0.1 (dashed line), and 0.01 (long dashed line), together with the one in the absence of microlensing (solid line). The lensing mass is $M_{\text{lens}} = 1.0M_{\odot}$.

only the disk brightening, but also substantial spectral deformation is produced by microlensing, when the angular separation is small (Rauch & Blandford 1991; Jaroszyński, Wambsganss & Paczyński 1992). The smaller the angular separation is, the larger becomes the modification of the

observed spectrum. In other words, the amplification factor depends on the frequency (wavelength) of the emitted photons. This gives rise to frequency-dependent, microlensing light curves (see §3.3). As for the optically thin disk, in contrast, there will not be large spectral modification by microlensing, but the flux is amplified over wide frequency ranges.

To understand such spectral properties, we divide the disk plane into three parts; $r \leq 10r_g$, $10r_g < r < 100r_g$, and $10^2r_g < r < 10^3r_g$, and plot the spectrum from each part of the disk, together with the integrated spectra, in figure 2.

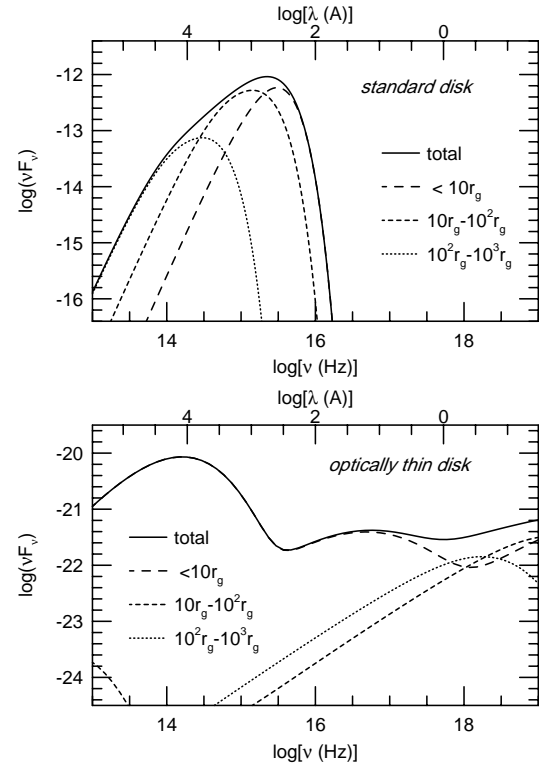


Fig. 2. Contribution to the total integrated spectra from different parts of disks for the cases of a standard (upper) and optically thin (lower) disk, respectively. Each figure displays the contributions from the inner region of $r \leq 10r_g$ (long dashed line), the intermediate region of $10r_g \sim 100r_g$ (dashed line), and the outer region of $10^2r_g \sim 10^3r_g$ (dotted line).

In the case of the optically thick accretion disk, photons emitted from different radii have different dominant frequencies because the local temperature of the disk has a strong radial dependence, $T \propto r^{-3/4}$ (Eq. [1]). For $u = 0.01$, therefore, the emission only from the inner, hottest part is strongly magnified, giving rise to a spectrum with one sharp peak at $\nu \sim 10^{15.3} \text{ Hz}$ ($\sim 1500\text{Å}$). Note that even without lensing the total spectrum has a peak at $\nu \sim 10^{15.3} \text{ Hz}$, but its low-frequency part has a smaller slope ($\nu F_{\nu} \propto \nu^{4/3}$) than that of blackbody radi-

ation ($\nu F_\nu \propto \nu^3$), thus a shoulder like feature extending to $\nu \sim 10^{14}$ Hz ($\sim 30000 \text{ \AA}$) being formed. This is because the outer cooler portions also contribute to the spectrum.

To help understanding such situation, we also plot the radial distribution of emitted photons with several wavelengths in figure 3. The upper panel of figure 3 shows

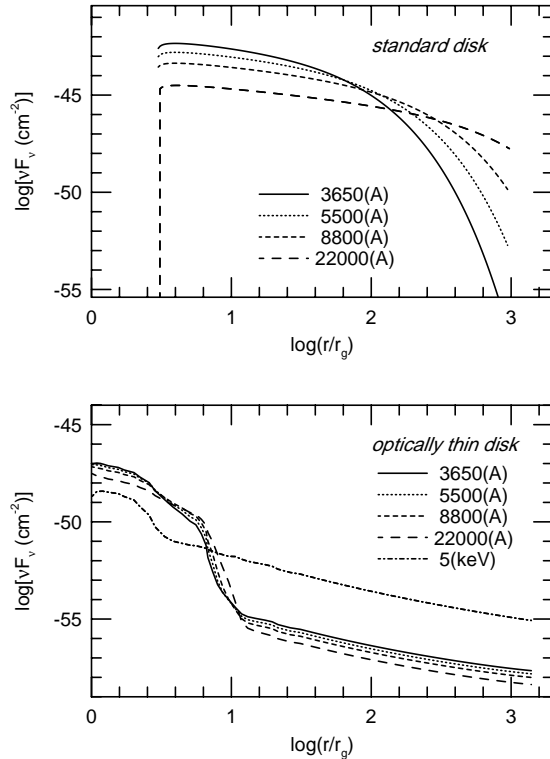


Fig. 3. The radial distribution of the emergent flux with several wavelengths for the case of a standard-type disk (upper) and an optically thin disk (lower), respectively. The adopted bands are U-band (3650 Å, by the solid line), V-band (5500 Å, by the dotted line), I-band (8800 Å, by dashed line), K-band (22000 Å, by long dashed line), and X-ray (5 keV, by the dot-dashed line).

rather gradual change of each flux over a wide spatial range. This reflects the fact that viscous heating and radiative cooling are balanced in the standard disk. Since the potential energy only gradually changes with the radius, so is the viscous heating rate and is the radiative cooling rate. Moreover, the lower a photon frequency is (or the longer the wavelength is), the wider becomes the parts of the disk which generate photons.

In the optically-thin accretion disk, on the other hand, the optical-UV flux is totally dominated by that from the inner region ($r \leq 10r_g$). The lower panel of figure 3 clearly shows that almost 100% of optical flux originates from the region inside $10r_g$, and that the contribution from the outer parts is smaller by several orders. This is possible in ADAF, since radiative cooling is no longer directly related

to the shape of the gravitational potential well (which has a rather smooth profile). The reason why optical flux is produced in a rather restricted region inside $10r_g$ is due to enhanced synchrotron emission in the vicinity of the black hole, where density and pressure (and thus magnetic pressure) are likely to be at maximum within the flow. Nearly irrespective of the u value, as a consequence, it is always the innermost region (within $10 r_g$) that dominates the entire disk spectrum. The amplification of the total emission just reflects that of the emission from the innermost parts. Therefore, the overall flux will be amplified by lensing without large spectral changes.

In X-ray ranges, in contrast, radiation originates from wider disk ranges; the contribution from the outer part at $100 - 1000r_g$ is not negligible at frequency of $f \sim 10^{18}$ (a few keV). Figure 3 also shows that X-rays are produced over a wider range. This is because of a high electron temperature, $T_e \sim 10^9 K$ maintained even at $r \sim 100r_g$ (see Manmoto et al. 1997). We can thus predict that small frequency dependence will be seen in X-ray ranges in this model.

Such quite different spectral behavior give rise to different light curves of different disk models.

3.3. Light curves

Using the results of the previous subsection, we now calculate the light curve during the microlensing events. We continuously change the angular separation between the lens and the center of the accretion disk (θ_d) according to

$$\theta_d = \theta_E \left[b^2 + \left(\frac{v_t t}{D_{ol} \theta_E} \right)^2 \right]^{1/2}, \quad (11)$$

and calculate the flux at each frequency, where b is the impact parameter (in the unit of θ_E), v_t is the transverse velocity of the lens and t is the time. Note that, v_t also includes the transverse velocity of the peculiar motion of the foreground galaxy relative to the source and the observer.

Figure 4 shows the microlensing light curves of optically thick (upper panel) and thin (lower panel) disks for the case with $(b, M_{\text{lens}}) = (0.01, 1.0 M_\odot)$. The light curve of the optically thin disk is still achromatic because of its flat temperature distribution, whereas the light curve of the optically thick disk shows strong frequency dependence.

Figure 3 is again useful to understand this chromaticity and achromaticity. Since flux distribution is similar among different optical fluxes in the case of optically thin disks, each optical flux is amplified in a similar way and thus the color does not change; i.e. achromatic feature appears. X-ray emitting region is wider than that of optical flux, small chromaticity may appear when we compare optical and X-ray light variations.

In an optically thick disk, conversely, low-energy photons are created in a wider spatial range, compared with

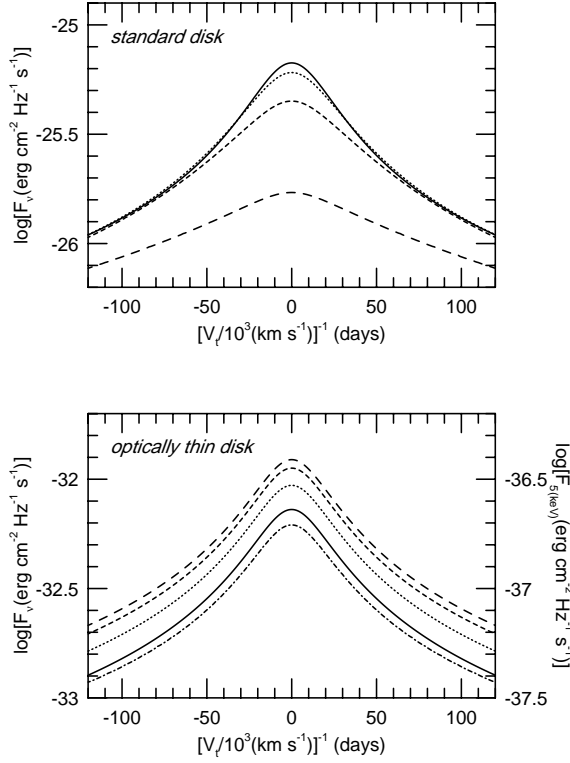


Fig. 4. The microlensed light curves of the standard disk (upper) and for the optically thin flow (lower). The parameters are $(b, M_{\text{lens}}) = (0.01, 1.0M_{\odot})$. The different type of lines correspond to the same as in figure 3.

high-energy photons. If the microlensing event occurs, therefore, low-energy emission will be the first to be amplified, followed by the significant amplification of high-energy emission. Note that each optical flux has the same level at the beginning (at -120 d) in the upper panel of figure 4, whereas a higher-energy optical flux is greater than that of a lower-energy flux in the intrinsic spectra in the absence of lensing (see figure 2). This indicates that the amplification of a lower-energy flux has already been appreciable at -120 d. This results in the color change; i.e. chromatic feature is produced.

3.4. Parameter dependence

Figure 5 shows the light curves for the case with one order smaller lensing mass and the same actual impact parameter ($b\theta_E$). Namely, $(b, M_{\text{lens}}) = [0.01(M_{\odot}/M_{\text{lens}})^{1/2}, 0.1M_{\odot}]$. We see that if the lens mass is small, the peak magnification is slightly reduced and the variability timescale is shorter, while the chromaticity of the standard disk still remains.

Next, in figure 6, we assign a larger impact parameter; $(b, M_{\text{lens}}) = (0.1, 1.0M_{\odot})$. In this case, not only the total amplification will become small but also chromaticity of standard disks no longer holds. Consequently, when we try to discriminate the disk structure, our success will

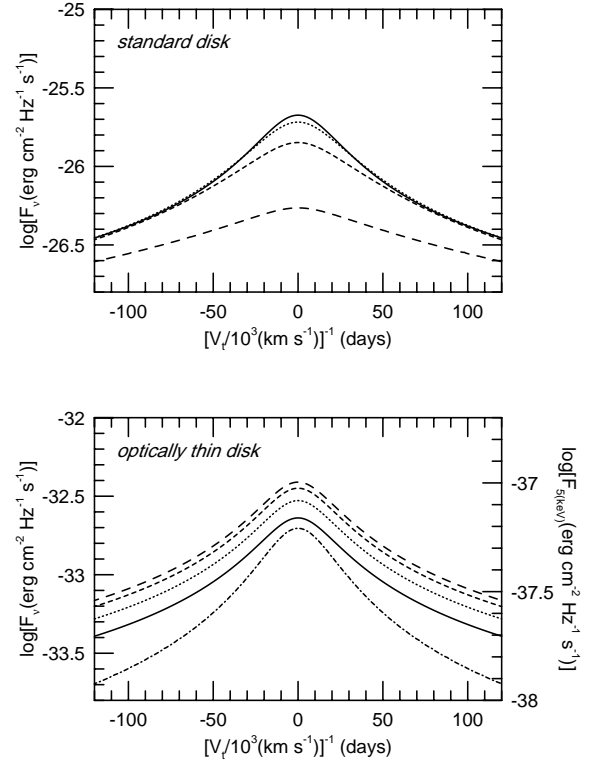


Fig. 5. Same as figure 4 but for the case with smaller lensing mass; $(b, M_{\text{lens}}) = [0.01(M_{\odot}/M_{\text{lens}})^{1/2}, 0.1M_{\odot}]$.

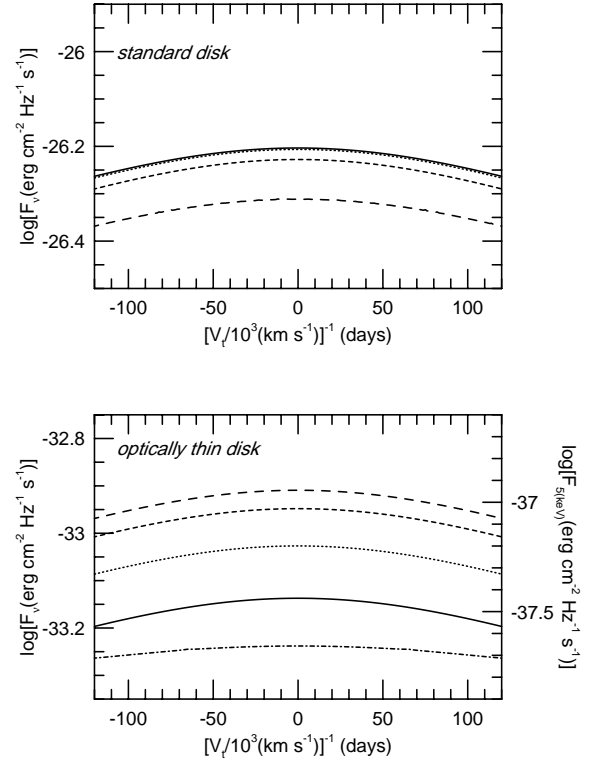


Fig. 6. Same as figure 4 but for the case with larger impact parameter; $(b, M_{\text{lens}}) = (0.1, 1.0M_{\odot})$.

depend not on whether the lens mass is large or not, but on whether the impact parameter is small or not. We will discuss this point later (in section 4).

Finally, figure 7 shows the dependence of the spectrum on the lens mass.

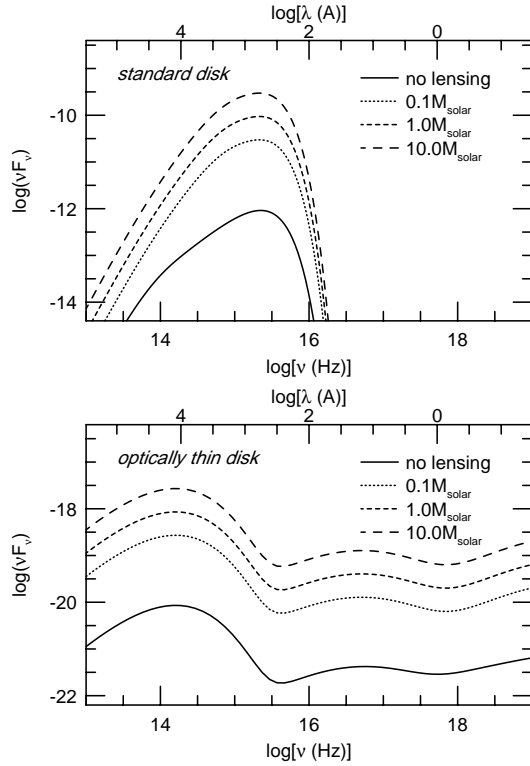


Fig. 7. Dependence of the microlensed light curves of the standard disk (upper) and the optically thin flow (lower) on the lensing mass, $M_{\text{lens}} = 0.1M_{\odot}$ (dotted line), $1.0M_{\odot}$ (dashed line), and $10.0M_{\odot}$ (long dashed line). The impact parameters are $0.01(M_{\odot}/M_{\text{lens}})^{1/2}$. The spectrum without microlensing is also plotted by the solid line.

The smaller the lens mass is, the sharper (or more narrow) the resulting shapes of the spectrum become. This is because when the lens mass is small, the Einstein-ring radius is small ($\theta_E \propto M_{\text{lens}}^{1/2}$, see Eq. [5]), so is the size of the region undergoing microlensing amplification. This reduces the total light amplification.

4. Discussion

We have demonstrated how spectral behavior and microlensing light curves change with time, depending on the disk structure. We considered two representative disk models: the standard-type disk emitting predominantly optical-UV photons, and the optically thin, advection-dominated flow (ADAF) producing a wide range of photons from radio to X- γ rays. Using the microlensing events,

we can distinguish the different structure of AGN accretion disks and map them in details.

At the peak of the microlensing event, the inner part of the accretion disk is strongly magnified (especially, when the impact parameter is small). Broad band photometry will be able to detect the color changes as shown in figure 4, thereby revealing the structure of AGN accretion disks. Fortunately, such observations do not require good time resolution, as long as a lens is located far from the observer.

To summarize the distinct properties of the two types of disks, we plot in figure 8 differences in the amplification factors at two different frequencies. Open and filled circles

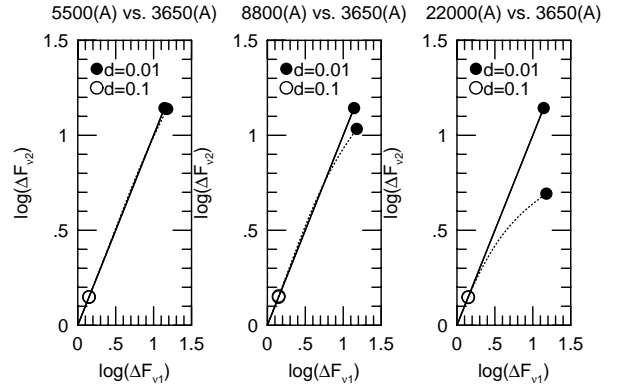


Fig. 8. Differences in the amplification factors at two different frequencies for the case of the standard disk (by the dotted line) and the optically thin flow (by the solid line), respectively. Two frequencies of these three panels are U-band and V-band (left panels), U-band and I-band (middle panels), and U-band and K-band (right panels), respectively. Open and filled circles represent the cases with $b = 0.1$ and $b = 0.01$, respectively. The lensing mass is assumed to be $M_{\text{lens}} = 1.0M_{\odot}$.

represent the cases with $b = 0.1$ and $b = 0.01$, respectively. The lensing mass is assumed to be $M_{\text{lens}} = 1.0M_{\odot}$. As the angular separation between the lens and the disk center (u) decreases, ΔF increases (thus the point moves in the upper right direction in figure 8). Obviously, the color changes are more pronounced in the right panel (between the U- and K-bands) than in the left panel (between the U- and V-bands), and for smaller impact parameters. We can easily discriminate the disk structure by comparing the optical and IR fluxes if $b \lesssim 0.03$.

As a first step to understand the microlensing phenomenon, we have considered microlensing by a single star in the present study. However, the microlensing events caused by a single lens, especially those with impact parameter $\leq 0.01\theta_E$, may not be frequent for the case of Q2237+0305. We thus need to evaluate the average time interval (Δt) between microlensing events with an impact parameter smaller than b . From Paczyński (1986), we find that $\langle \Delta t \rangle$ is proportional to b^{-1} . On the other hands, mi-

crolensing does occur in Q 2237+0305 at a rate of at least one event per year, i.e. $\langle \Delta t \rangle \sim 1\text{yr}$ (Corrigan et al. 1991; Houde & Racine 1994). Hence, microlensing events which we are interested in occurs every 10 yr ($b = 0.1$) to 100 yr ($b = 0.01$).

To conclude, microlensing events with such a small impact parameter may not be frequent, but once the microlensing with a small impact parameter occurs, a large light amplification is expected. We have demonstrated that an optically thick accretion disk exhibits more curious features in its spectral shape than an optically thin accretion disk.

The single-lens model as adopted in this paper is a good approximation, unless the apparent separations among lens stars are appreciably smaller than the radius of the Einstein ring in the source plane. But, we should note that the images of Q2237+0305 could be subject to microlensing by multiple stars of the foreground galaxy (e.g., $\tau = 0.4 \sim 0.7$ from Rix, Schneider, & Bahcall 1992). That is, we must consider, as a next step, the microlensing events caused by ‘caustics’ which is produced by multiple microlensing. Such events may occur more frequently with shorter duration and steeper magnification (Wambsganss & Kundić 1995). Light curves by the caustics will show even more interesting features than the present case (Schneider & Weiss 1986). This will be done in a subsequent paper.

Finally, recent high-resolution observations, including those from *HST*, have revealed circumnuclear starburst regions in AGNs (see Umemura, Fukue & Minesgige 1997, and references therein). If starburst region exists around an accretion disk, microlensing event of AGN will make an interesting light curve; large-amplitude, short timescale variation (on a few months) caused by the microlensing of the accretion disk will be superposed on more gradual light variation (over a year) caused by the microlensing of starburst region (see figure 9). Thus, long-term monitoring may provide a possible tool to elucidate the extension of circumnuclear starbursts.

This diagnostic method for the central region of AGN can be used in other source (e.g., MG0414+0534, PG1115+080, and so called ‘clover leaf’, H1413+117 etc.).

Acknowledgements. We thank Joachim Wambsganss for valuable comments. This work was supported in part by the Japan-US Cooperative Research Program which is founded by the Japan Society for the Promotion of Science and the US National Science Foundation, and by the Grants-in Aid of the Ministry of Education, Science, and Culture of Japan, 08640329 (S.M.).

References

Abramowicz, M.A., Chen, X., Kato, S., Lasota, J.-P., & Regev, O. 1995, *ApJ*, 438, L37
 Blandford, R.D., & Hogg, D.W. 1995, in *IAU Symp.* 173, *Astrophysical Applications of Gravitational Lensing*, ed. Kochanek, C.S., & Hewitt, J.N. (Dordrecht:Kluwer), 355

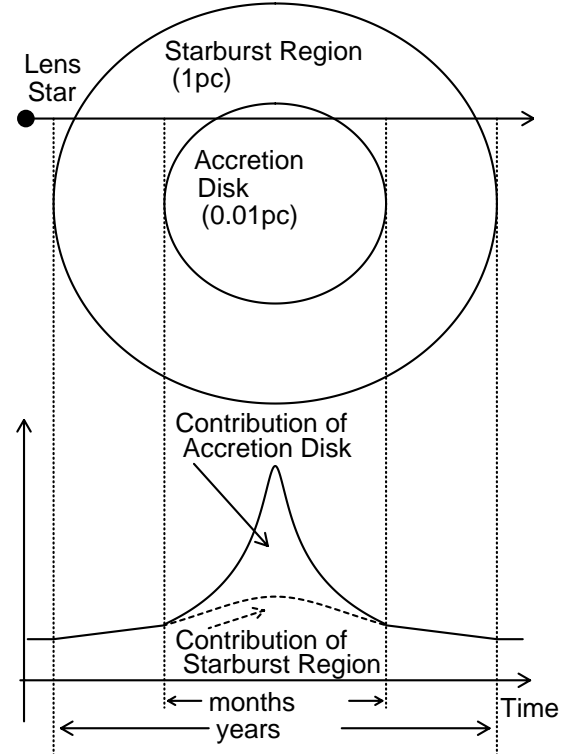


Fig. 9. Schematic view of a microlensing event of an AGN disk and circumnuclear starburst regions.

Chang, K., & Refsdal, S. 1984, *A&A*, 132, 168
 Corrigan, R.T. et al. 1991, *AJ*, 102, 34
 Grieger, B., Kayser, R., & Refsdal, S. 1988, *A&A*, 194, 54
 Houde, M., & Racine, R. 1994, *AJ*, 107, 466
 Huchra, J., Gorenstein, M., Horine, E., Kent, S., Perley, R., Shapiro, I. I., & Smith, G. 1985, *AJ*, 90, 691
 Irwin, M.J., Webster, R.L., Hewitt P.C., Corrigan R.T., & Jędrzejewski, R.I. 1989, *AJ*, 98, 1989
 Jaroszyński, M., Wambsganss, J., & Paczyński, B. 1992, *ApJ*, 396, L65
 Kundić, T. et al. 1997, *ApJ*, 482, 75
 Manmoto, T., Mineshige, S., & Kusunose, M. 1997, *ApJ*, 489, 791
 Narayan, R., & Bartelmann, M. 1996, *astro-ph/9606001*
 Narayan, R., & Yi, I. 1995, *ApJ*, 452, 710
 Paczyński, B. 1986, *ApJ*, 304, 1
 Rauch, K.P., & Blandford, R.D. 1991, *ApJ*, 381, L39
 Rix, H.-W., Schneider, D.P., & Bahcall, J.N. 1992, *AJ*, 104, 959
 Schneider, P., & Weiss, A. 1986, *A&A*, 164, 237
 Shakura, N.I., & Sunyaev, R.A. 1973, *A&A*, 24, 337
 Umemura, M., Fukue, J., & Mineshige, S. 1997, *ApJ*, 479, L97
 Wambsganss, J., & Kundić, T. 1995, *ApJ*, 450, 19
 Wambsganss, J., & Paczyński, B. 1991, *AJ*, 102, 864
 Wambsganss, J., Paczyński, B., & Schneider, P. 1990, *ApJ*, 358, L33
 Zheng, W., Kriss, G.A., Telfer, R.C., Grimes, J.P., & Davidsen, A.F. 1997, *ApJ*, 475, 469

This article was processed by the author using Springer-Verlag
L^AT_EX A&A style file *L-AA* version 3.